Polyhedron 150 (2018) 1–9

Contents lists available at ScienceDirect

Polyhedron

journal homepage: www.elsevier.com/locate/poly

Polyhedron Report # XX

Bis-tris propane as a flexible ligand for high-nuclearity complexes

Mark Murrie

WestCHEM, School of Chemistry, University of Glasgow, University Avenue, Glasgow G12 8QQ, UK

ARTICLE INFO

Article history:
Received 6 March 2018
Accepted 30 April 2018
Available online 9 May 2018

Keywords:
Bis-tris propane
Polydentate ligands
High nuclearity complexes
Heterometallic complexes
Magnetic properties

ABSTRACT

Polymetallic complexes can be assembled using a wide array of polydentate ligands that give an almost unlimited toolbox to prepare new molecular architectures with fascinating structures and interesting magnetic properties. Bis-tris propane is one such a polydentate ligand that has been used to prepare homo- (3d or 4f) and heterometallic (3d/3d′ or 3d/4f) complexes, ranging from simple complexes such as $\{Ni_4\}$ to spectacular 3d/3d′ $\{Cu_8Zn_8\}$ or $\{Mn_{18}Cu_6\}$ complexes. It shows a flexibility in binding mode, utilizing up to six of its potential ligand donor atoms and displaying multiple levels of deprotonation, able to bridge up to six metal ions. The ligand has a particular affinity for binding 3d ions such as Cu(II) or Co(III) in heterometallic syntheses and this can provide a flexible structure-directing effect. This concept has been exploited to prepare new heterometallic 3d/3d′ complexes that display interesting levels of complexity; 3d/4f complexes such as $\{Cu_3Tb_2\}$ that show single-molecule magnet behavior where superexchange interactions quench quantum tunneling of the magnetization, or $\{Co_3Gd_3\}$ where the magnetocaloric properties arise by using Bis-tris propane to separate the Gd(III) ions and weaken Gd(III)...Gd(III) interactions.

Contents

1. Introduction

The synthesis and characterization of polymetallic complexes remains a hot topic within the area of inorganic chemistry [1–3]. Current areas of interest relate to single-molecule magnets (SMMs) [4,5]; magnetic refrigerants [6]; qubits [7]; complexes with toroidal moments [8]; the magnetic behavior of high symmetry systems [9–11]; magnetic bistability on surfaces [12]; mimics of the oxygen evolution center in photosystem II [13], and water oxidation electrocatalysis [14]; MRI contrast agents [15] and as precursors for magnetic nanoparticles [16], or lithographic resists [17]. However, the synthetic challenges involved in isolating such systems [18] and the search for emergent properties in larger and larger systems is also a major driving force [19–23]. We have a long-standing interest in the use of polydentate ligands [24] to direct the assembly of homo- and heterometallic complexes and in particular a series of structurally related ligands containing the Tris unit {(Tris = 2-amino-2-(hydroxymethyl) propane-1,3-diol} [25,26] such as Bis-tris {2-[bis(2-hydroxyethyl) amino]-2-(hydroxymethyl) propane-1,3-diol} [27–29]. This research led us to investigate Bis-tris propane $\{H_6L$ = 2,2′-(propane-1,3-diyldiimino)bis[2-(hydroxymethyl)propane-1,3-diol} as a ligand. The skeleton of Bis-tris propane provides high flexibility and includes a $\{N_2O_6\}$ unit containing multiple binding sites and hence, excellent potential as a bridging ligand (Chart 1). Bis-tris propane is widely used as a biological buffer, and is especially useful as an additive for screening

E-mail address: mark.murrie@glasgow.ac.uk

https://doi.org/10.1016/j.poly.2018.04.038
0277-5387/

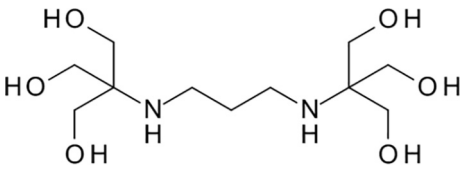

Chart 1. Bis-tris propane (H_6L).

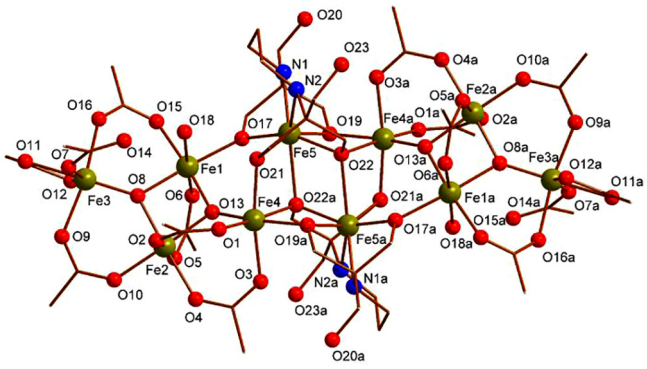

Fig. 1. Structure of $[Fe_{10}O_4(H_2L)_2(OAc)_{14}(H_2O)_2]$ (ball and stick representation with Fe, gold; O, red; N, blue; C, brown; H omitted for clarity). Reprinted with permission from Ref. [34]. Copyright 2008 American Chemical Society. (Color online.)

protein crystallization conditions. The possibility of buffer interference by 3d metal complexation has been studied [30]. More recently, Bis-tris propane has been employed to lower the redox potential of the Mn(II)/Mn(III) couple in the study of electron transfer processes in native anoxygenic bacteria [31], as a ligand in the Ce^{IV}-assisted hydrolysis of phosphatidylcholine liposomes [32] and when dissolved in DMSO it has been studied for CO_2 capture via amine scrubbing [33].

2. Homometallic complexes

The first complexes containing the Bis-tris propane ligand were polymetallic iron(III) and manganese(II/III) complexes [34]. Our route into the iron(III) chemistry was through the well-established oxo-centered Fe_3 triangle precursor methodology [35], in this case reacting the disodium salt Na_2H_4L with $[Fe_3O(OAc)_6(H_2O)_3]Cl$ in MeCN at ambient temperature to yield $[Fe_{10}O_4(H_2L)_2(OAc)_{14}(H_2O)_2]$ (**1**).

The complex contains two distorted Fe_4 butterfly units linked together by two central $\{Fe(H_2L)\}^-$ units (Fig. 1). All iron centers within the Fe_4 butterfly units have a distorted octahedral coordination sphere, whereas Fe5 has a less common distorted monocapped trigonal prismatic geometry where the trigonal prism is formed from the $\{N_2O_4\}$ ligand donor set. The ligand is present in one μ_5-binding mode (Chart 2) and two ligand arms remain protonated and unbound (O20, O23), hydrogen bonding to acetate ligands on adjacent Fe_{10} molecules. Next we turned to mixed-valence manganese complexes, finding success by using a combination of $Mn(acac)_2$ and $Mn(OAc)_2$ as precursors with H_6L and triethylamine in MeOH at ambient temperature to yield $[Mn^{III}_2Mn^{II}_4(H_2L)_2(acac)_4(OAc)_2(MeOH)_2]$ (**2**).

As seen in complex **1**, the Bis-tris propane ligand links together smaller sub-units: in **2**, these are Mn(II) dimers (Fig. 2). Mn1 and Mn3 are divalent with a distorted octahedral geometry, whereas

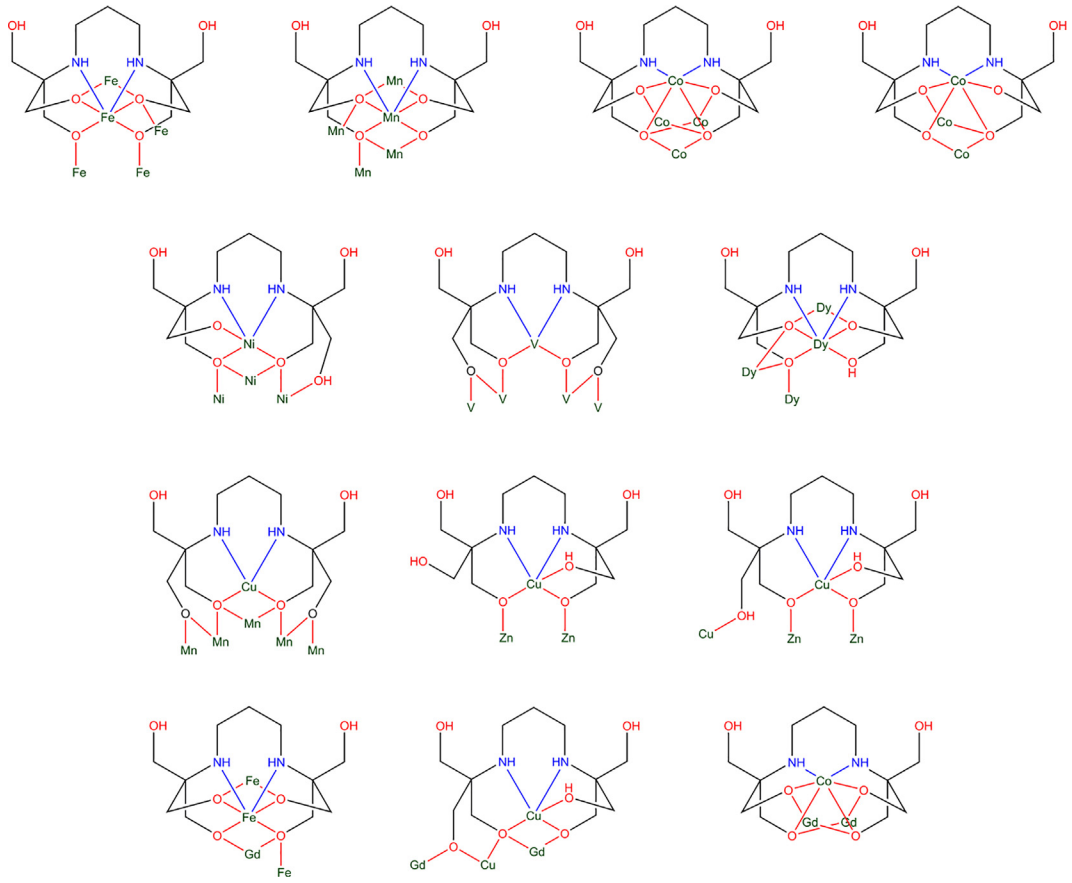

Chart 2. The ligand binding modes in homo- and heterometallic complexes.

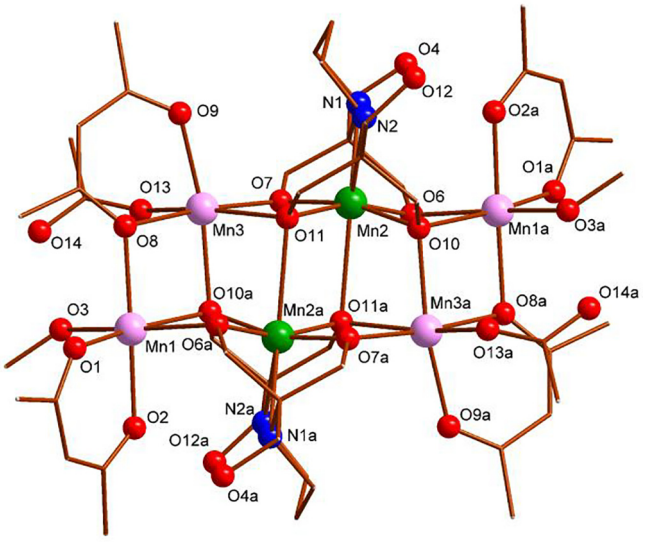

Fig. 2. Structure of $[Mn^{III}_2Mn^{II}_4(H_2L)_2(acac)_4(OAc)_2(MeOH)_2]$ (ball and stick representation with Mn(III) green; Mn(II), pink; O, red; N, blue; C, brown; H omitted for clarity). Reprinted with permission from Ref. [34]. Copyright 2008 American Chemical Society. (Color online.)

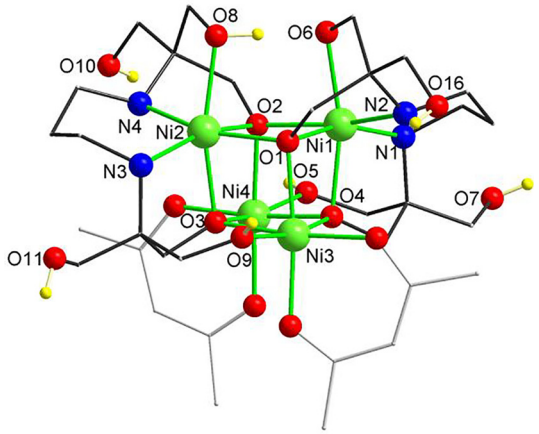

Fig. 3. Structure of $[Ni_4(H_4L)(H_3L)(acac)_2]^+$ (Ni, green; N, blue; O, red; C, black rods for Bis-tris propane ligand or grey rods for acac; H, yellow). H atoms are shown only for the Bis-tris propane ligand OH groups that remain protonated. Reproduced from Ref. [36] by permission of The Royal Society of Chemistry (2011). (Color online.)

trivalent Mn2 possesses an unusual distorted mono-capped trigonal prismatic geometry where the trigonal prism is formed from the $\{N_2O_4\}$ ligand donor set as seen in complex **1**. Again, the ligand is present in one binding mode (Chart 2) where two unbound ligand arms remain protonated (O4, O12) and form hydrogen bonds to adjacent complexes in the crystal lattice.

The magnetic properties of complexes **1** and **2** are dominated by intramolecular antiferromagnetic superexchange interactions between the metal centers (Table 1). Following this observation, we started to think about the possibility of synthesizing heterometallic complexes with Bis-tris propane, by using the $\{N_2O_4\}$ encapsulating motif to help discriminate between different metal ions. However, before this, we targeted nickel and cobalt leading to Ni_4 and Co_5 complexes [36]. Employing a similar strategy to that used above for complex **2**, reaction of $Ni(OAc)_2$ and $Ni(OAc)_2$ with H_6L and diethylamine in MeOH at ambient temperature yields, after layering with Et_2O, $[Ni_4(H_4L)(H_3L)(acac)_2][OAc]$ (**3**).

All four Ni(II) centers in complex **3** have a distorted octahedral geometry and two (Ni1 and Ni2) are ligated in an $\{N_2O_4\}$ environment from the Bis-tris propane ligand (Fig. 3). Each Bis-tris propane ligand displays the same binding mode but exists in either the di- or tri-anionic form (shown as H_3L^{3-} in Chart 2). The 'extra' ligand OH proton lies along the short O8-H8-O6 hydrogen bond (2.48 Å). Reaction of $Co(acac)_2$ with H_6L in $MeOH/CH_2Cl_2$ at ambient temperature yields, after layering with Et_2O, $[Co^{II}_3Co^{III}_2(H_2L)_2(acac)_3(MeOH)][Co^{II}(acac)_3]$ (**4**).

Complex **4** is a mixed-valence pentametallic cobalt complex (Fig. 4). The cobalt(II) centers have a distorted $\{CoO_6\}$ octahedral coordination sphere and form a coupled unit, while the remaining two cobalt centers (Co3 and Co6) are trivalent and are each encapsulated by one H_2L^{4-} ligand with an $\{N_2O_4\}$ ligand donor set. The H_2L^{4-} ligand displays two very similar binding modes, encapsulating a Co(III) center and further binding to either two (Co4, Co5) or

Table 1
Summary of magnetic properties.

Compound	Magnetic properties
$[Fe_{10}O_4(H_2L)_2(OAc)_{14}(H_2O)_2]$ (**1**)	$S = 0$ ground state
$[Mn_6(H_2L)_2(acac)_4(OAc)_2(MeOH)_2]$ (**2**)	$S = 0$ ground state, low-lying states
$[Ni_4(H_4L)(H_3L)(acac)_2][OAc]$ (**3**)	$S = 4$ ground state ($J_1 = 10.8$ cm^{-1}, $J_2 = 2.4$ cm^{-1})
$[Co_5(H_2L)_2(acac)_3(MeOH)][Co^{II}(acac)_3]$ (**4**)	Ferromagnetic coupling
$[NMe_4]_4[V_7O_{11}(OMe)(SO_4)_3(H_2L)]$ (**5**)	*Not reported*
$[Dy_4(H_3L)_2(OAc)_6]$ (**6**)	Two relaxation regimes: $\Delta E/k_B = 44$ K and 107 K
$[Cu(H_6L)Cl]Cl$ (**7**)	*Not reported*
$[Mn_{18}Cu_6O_{14}(H_2L)_6Cl_2(H_2O)_6]Cl_6$ (**8**)	Antiferromagnetic coupling, low-lying states
$[Mn_{18}Cu_6O_{14}(H_2L)_6Cl_6]Cl_2$ (**9**)	Antiferromagnetic coupling, low-lying states
$[Cu_2Zn_2(H_4L)_2(OAc)_2Cl_2]$ (**10**)	Antiferromagnetic coupling, $J = -11.5$ cm^{-1}
$[Cu_8Zn_8(OH)_8(H_4L)_8](Cl)_2(ClO_4)_6$ (**11**)	Antiferromagnetic coupling, $J = -1.23$ cm^{-1}
$[Fe_6Y_2(O)_2(H_2L)_2(Piv)_{12}]$ (**12**)	$S = 5$ ground state
$[Fe_6Gd_2(O)_2(H_2L)_2(Piv)_{12}]$ (**13**)	Fe_6 core weakly coupled to two Gd^{III} ions
$[Fe_6Dy_2(O)_2(H_2L)_2(Piv)_{12}]$ (**14**)	Onset of slow relaxation
$[Fe_6Tb_2(O)_2(H_2L)_2(Piv)_{12}]$ (**15**)	Onset of slow relaxation
$[Gd_2Cu_3(H_3L)_2(OAc)_6]$ (**16**)	$J_{Cu\ldots Gd} = +1.8$ cm^{-1}, $J_{Cu\ldots Cu} = +69.7$ cm^{-1}
$[Tb_2Cu_3(H_3L)_2(OAc)_6]$ (**17**)	$\Delta E/k_B = 21.4$ K
$(NMe_4)_2[Gd_2Cu_3(H_3L)_2(NO_3)_8(EtOH)_2]$ (**18**)	$J_{Cu\ldots Gd} = +1.9$ cm^{-1}, $J_{Cu\ldots Cu} = +16.7$ cm^{-1}
$(NMe_4)_2[Tb_2Cu_3(H_3L)_2(NO_3)_7(MeOH)_2](NO_3)$ (**19**)	$\Delta E/k_B = 36.0$ K
$(NMe_4)_2[Dy_2Cu_3(H_3L)_2(NO_3)_7(MeOH)_2](NO_3)$ (**20**)	$\Delta E/k_B = 23.9$ K
$(NMe_4)_2[Ho_2Cu_3(H_3L)_2(NO_3)_7(MeOH)_2](NO_3)$ (**21**)	$\Delta E/k_B = 17.2$ K
$(NMe_4)_2[Er_2Cu_3(H_3L)_2(NO_3)_7(MeOH)_2](NO_3)$ (**22**)	$\Delta E/k_B = 14.8$ K
$[Co_3Gd_3(H_2L)_3(acac)_2(OAc)_4(H_2O)_2]$ (**23**)	$\Delta T_{ad} = 10.7$ K at $T = 1.5$ K for $\Delta B = (7–0)$ T

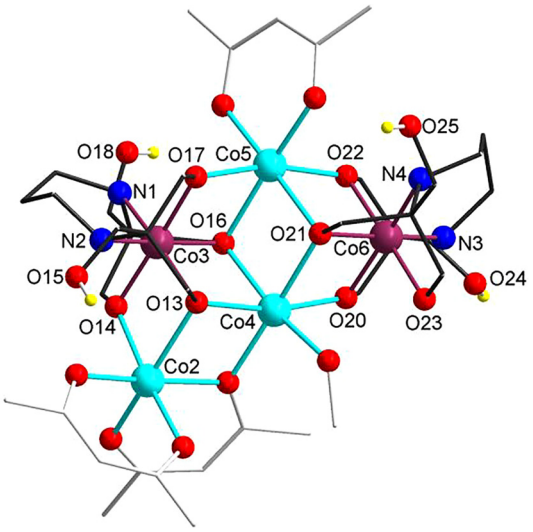

Fig. 4. Structure of $[Co^{II}_3Co^{III}_2(H_2L)_2(acac)_3(MeOH)]^+$ (Co(II), cyan; Co(III), purple; N, blue; O, red; C, black rods for Bis-tris propane ligand or grey rods for acac; H, yellow). H atoms are shown only for the Bis-tris propane ligand OH groups that remain protonated. Reproduced from Ref. [36] by permission of The Royal Society of Chemistry (2011). (Color online.)

three (Co2, Co4, Co5) Co(II) centers (Chart 2). Complex **4** was the first complex that contains a fragment of the larger more typical planar $\{Co_7\}$ disc structures [37,25]. The magnetic properties of complexes **3** and **4** are dominated by ferromagnetic superexchange interactions (for **3**, $S = 4$) although neither complex displays slow magnetic relaxation down to 1.8 K. Bis-tris propane has been used recently as a bridging ligand in a hybrid polyoxovanadate complex $[NMe_4]_4[V^{V}V^{IV}_6O_{11}(OMe)(SO_4)_3(H_2L)]$ (**5**) [38]. Complex **5** was prepared solvothermally from $VOSO_4$, NMe4OH and H_6L in MeOH (at 125 °C for 24 h). The H_2L^{4-} ligand encapsulates one V(IV) center and bridges to a further four V centers via four μ-bridging O donors (Chart 2).

Although dinuclear lanthanide complexes were proposed in solution in 2001 [39], there is only one example of a polymetallic Bis-tris propane lanthanide complex $[Dy_4(H_3L)_2(OAc)_6]$ (**6**), which is prepared solvothermally (at 100 °C for 3 days) from $Dy(OAc)_3$, Bis-tris propane and LiOH in EtOH (see Fig. 5). The structure is a planar Dy_4 parallelogram where each Bis-tris propane ligand encapsulates a central Dy(III) with an N_2O_4 donor set and further bridges to the three other Dy(III) centers (Chart 2). A co-ligand is required to isolate a polymetallic complex as seen in the assembly of the 3d complexes above. Complex **6** displays slow magnetic relaxation below 20 K in ac susceptibility measurements with two separate relaxation regimes, corresponding to the low-temperature and the high-temperature region. These have been analyzed as Orbach relaxation processes with $U_{eff} = 44$ K ($\tau_0 = 1.0 \times 10^{-6}$ s) and $U_{eff} = 107$ K ($\tau_0 = 2.0 \times 10^{-7}$ s) and are likely to be attributable to the individual Dy^{3+} ions, which have two distinct coordination environments (monocapped square-antiprism and distorted square-antiprism) rather than the weakly coupled Dy_4 unit.

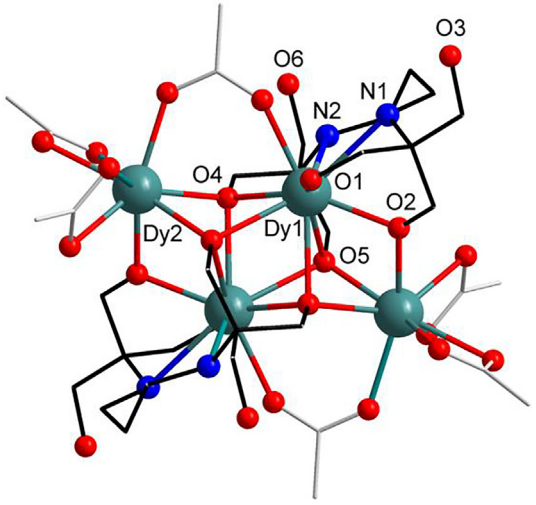

Fig. 5. Structure of $[Dy_4(H_3L)_2(OAc)_6]$ (Dy(III), teal; N, blue; O, red; C, black rods for Bis-tris propane ligand or grey rods for acetate; H atoms omitted for clarity). Image created from the crystallographic information file (CIF) from the Cambridge Structural Database (CSD) Refcode: OFUXEU. (Color online.)

3. Heterometallic 3d/3d' complexes

The use of two, or more, different metal ions to assemble large heterometallic complexes is a considerable synthetic challenge [19,40,41]. However, the potential rewards are significant, as there is a real possibility of control/design over the individual parameters that contribute to the overall molecular properties. In 2011, we initiated a program to utilize Bis-tris propane in the development of a step-by-step self-assembly synthetic approach to heterometallic complexes to take advantage of the encapsulating binding motif. We found that this binding pocket was an excellent fit for the copper(II) ion and this key observation allowed us to begin to develop the heterometallic chemistry of the ligand. We were able to employ a pre-formed Cu^{II} Bis-tris propane complex, which contains multiple, latent hydroxyl binding sites, to target the trapping and encapsulation of an inner metal-oxo core. The choice of Cu^{II} as the central ion increases the flexibility of the strategy further, due to its range of typical coordination environments from [4] to [4 + 2]. We were delighted that two of the first heterometallic complexes that we isolated using this strategy contained a 'core–shell' $\{Mn_{18}Cu_6\}$ complex, where the Cu^{II} precursors encapsulate a hexacapped-cuboctahedral manganese oxide $\{Mn^{III}_{12}Mn^{II}_6O_{14}\}$ nanocluster [42].

Firstly, the Cu^{II} center is enclosed forming the precursor complex [Cu(H_6L)Cl]Cl (**7**) in almost quantitative yield. Complex **7** is then used as a precursor to generate the heterometallic complexes: addition of base to a solution of **7**, followed by addition of $MnCl_2$ leads to the formation of $[Mn_{18}Cu_6O_{14}(H_2L)_6Cl_2(H_2O)_6]Cl_6$ (**8**) using NMe_4OH/EtOH or $[Mn_{18}Cu_6O_{14}(H_2L)_6Cl_6]Cl_2$ (**9**) (Fig. 6) using NEt_3/MeOH. Pre-formation of the Cu^{II} complex and the use of heat in the reactions appears to be essential. As an aside, in 2017 the related complex [Cu(H_5L)(N_3)] was reported as an efficient homogeneous catalyst for the mild oxidation (using aqueous H_2O_2) of C_5–C_8 cycloalkanes [43]. The structure of these cationic complexes is based upon a $\{Mn^{III}_{12}Mn^{II}_6O_{14}\}^{20+}$ core, encapsulated by six $\{Cu(H_2L)\}^{2-}$ groups. Each H_2L^{4-} ligand displays the same μ_6-binding mode and each Cu^{II} center is bridged to three manganese centers via two ligand alkoxide arms (Chart 2). The Mn^{III} centers describe a cuboctahedron, capped on each square face by a Mn^{II}, forming a giant octahedron. Six faces of this giant octahedron are capped by a Cu^{II} center, where the Cu^{II} ions describe a further octahedron, twisted with respect to the $\{Mn^{II}_6\}$ octahedron, giving a remarkable level of self-assembly: polyhedral shells of expanding size describing Archimedean $\{Mn^{III}_{12}\}$ < Platonic $\{Mn^{II}_6\}$ < Platonic $\{Cu^{II}_6\}$ solids. Each H_2L^{4-} ligand in **8** and **9** displays a μ_6-binding mode encapsulating one Cu(II) and bridging three Mn(II) and two Mn(III) centers. The core structure is largely the same, but each Mn(II) center is equivalent in **9** and has a terminal chloride ligand (*cf.* either Cl^- or H_2O in **8**) and complex **9** has a more compact core with higher symmetry (S_6). Furthermore, in **9** the second axial Cu(II) position (O73) is occupied

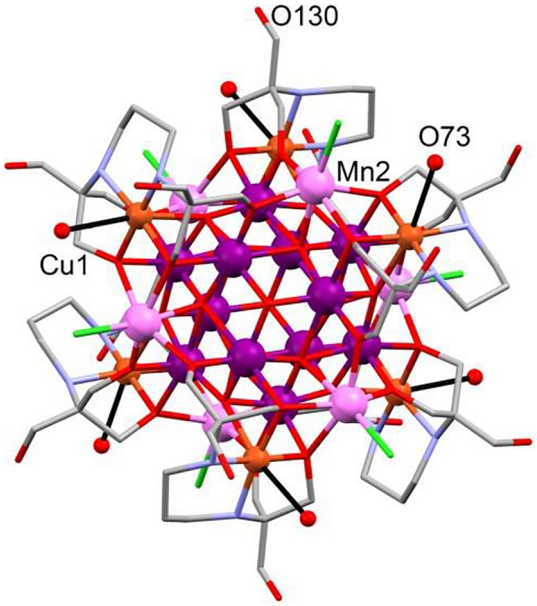

Fig. 6. Structure of $[Mn_{18}Cu_6O_{14}(H_2L)_6Cl_6]^{2+}$ viewed along the threefold axis. Mn^{III}, purple; Mn^{II}, pink; Cu^{II}, bronze; Cl, green; O, red; N, blue; C, grey (H atoms omitted for clarity). Bonds to oxygen atoms of neighboring clusters, utilized in forming a 3-D net are shown as solid black lines. Reprinted with permission from Ref. [42]. Copyright 2013 Wiley-VCH. (Color online.)

by the oxygen atom of a CH_2OH ligand arm on an adjacent molecule and each $\{Mn_{18}Cu_6\}$ cluster is connected to six nearest neighbor clusters creating a 3D network.

Interestingly, the $\{Mn^{III}_{12}\}$ core structure of the $\{Mn_{18}Cu_6\}$ complexes is related to the smaller Mn-oxo clusters, $[Mn^{IV}Mn^{III}_6Mn^{II}_6O_8(OEt)_6(O_2CPh)_{12}]$ [44] and $[Mn^{II}Mn^{III}_{12}O_8(Cl)_6(\text{tert-butyl-}PO_3)_8]$ [45] where the central position is occupied by a Mn^{IV} or a Mn^{II} cation, respectively (*cf.* empty cavity in **8** and **9**). The magnetic behavior of both complexes is dominated by antiferromagnetic coupling and magnetization *vs.* field data suggests a large number of excited states with similar energies, and a poorly defined ground state. We extended this synthetic approach recently to the related Edte ligand (H_4Edte = 2,2′,2″,2‴-(1,2-ethanediyldinitrilo)tetraethanol) [46,47], producing $[Mn^{III}_{10}Cu^{II}_5O_8(O_2CPh)_8(HEdte)_4(H_2O)_4][NO_3]_4$ a rare example of a heterometallic Mn/Cu system featuring Mn ions exclusively in the 3+ oxidation state [48].

To try to reduce the number of antiferromagnetic interactions in the Cu/Mn systems, and therefore increase the magnitude of the spin ground state, we proposed a strategy based on the replacement of the paramagnetic Cu(II) centers by diamagnetic Zn(II) ions. During the development of this strategy, we investigated the chemistry of the Bis-tris propane ligand in the formation of Cu/Zn heterometallic complexes. The reaction between H_6L, Cu$(OAc)_2$ and $ZnCl_2$ in MeOH with heating yields, after layering with Et_2O, $[Cu_2Zn_2(H_4L)_2(OAc)_2Cl_2]$ (**10**) [49]. However, when a mild base was added to a combination of H_6L, Cu$(ClO_4)_2$ and $ZnCl_2$ under analogous conditions to the synthesis of **10**, the complex $[Cu_8Zn_8(OH)_8(H_4L)_8](Cl)_2(ClO_4)_6$ (**11**) was obtained, which contains an unprecedented double-concentric ring structure.

The structure of **10** comprises two {Cu(H_4L)} units and two distorted tetrahedral Zn(II) ions that are linked by the two doubly deprotonated H_4L^{2-} ligands (Fig. 7). Each H_4L^{2-} ligand is coordinated to one Cu(II) center through two O- and two N-donor atoms in a [4 + 1] quasi-square-based pyramidal environment (Chart 2). One of the residual hydroxyl groups of H_4L^{2-} fills the axial position of the penta-coordinated Cu(II) centers; the three remaining ligand arms are uncoordinated. The structure of the $[Cu_8Zn_8(OH)_8(H_4L)_8]^{8+}$ complex in **11** consists of eight Cu(II) ions and eight Zn(II)

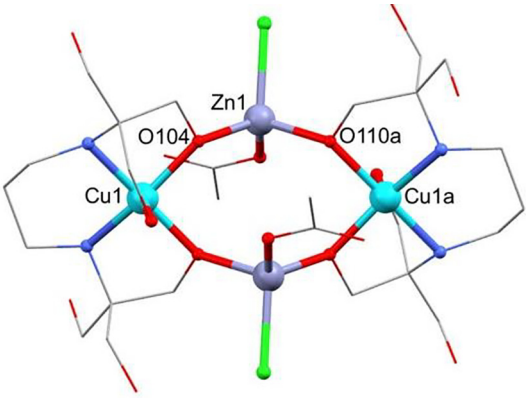

Fig. 7. Structure of $[Cu_2Zn_2(H_4L)_2(OAc)_2Cl_2]$. C, grey; Cl, green; Cu, turquoise; N, blue; O, red; Zn, lavender; H omitted for clarity. Reproduced from Ref. [49] published by The Royal Society of Chemistry (2015). (Color online.)

ions linked by hydroxide and H_4L^{2-} bridging ligands, adopting an unusual "double-concentric ring" structure (Fig. 8). The external ring is formed by {Cu(H_4L)} units, whereas the internal one is composed of Zn(II) centers and hydroxide ligands. Each Cu(II) center is coordinated to two H_4L^{2-} ligands through O- and/or N-donor atoms: one of the H_4L^{2-} ligands acts as a chelating ligand (see Chart 2 and Fig. 8 right) and the second, which is coordinated to the neighboring Cu(II) ion, completes the coordination sphere, leading to a [4 + 2] distorted octahedral environment. The alkoxide arms of the chelating H_4L^{2-} units also act as bridges between the Cu(II) ion and two Zn(II) ions; the remaining hydroxyl arms are unbound. Antiferromagnetic coupling between Cu(II) ions ($J = -11.5\ cm^{-1}$ in **10** and $J = -1.23\ cm^{-1}$ in **11** with $\hat{H} = -2J$ notation) is observed in both complexes, despite the long distances between paramagnetic metal centers, due to the involvement of diamagnetic Zn(II) ions in the magnetic exchange pathway.

4. Heterometallic 3d/4f complexes

The combined use of 3d/4f ions a good design strategy for single-molecule magnets, as certain lanthanide ions can provide the essential magnetic anisotropy and the 3d-4f exchange interaction can help to suppress Quantum Tunneling of the Magnetization (QTM) [50,51]. The first 3d/4f Bis-tris propane complexes were reported in 2015 with Fe(III) as the 3d center [52]. The complexes $[Fe_6Ln_2(O)_2(H_2L)_2(Piv)_{12}]$ where Ln = Y (**12**), Gd (**13**), Dy (**14**), Tb (**15**) are prepared from reaction of the oxo-centered triangle

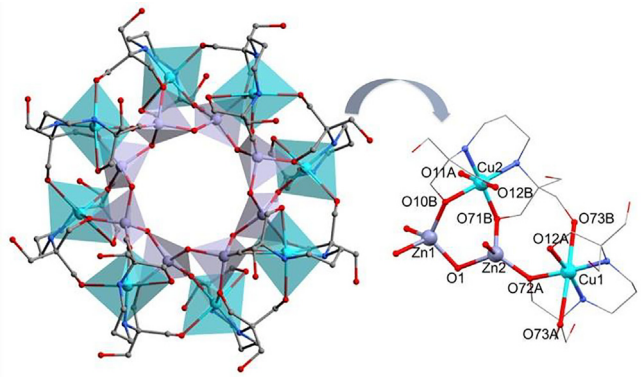

Fig. 8. Structure of $[Cu_8Zn_8(OH)_8(H_4L)_8]^{8+}$ (left) and detail (right). C, grey; Cu, turquoise; N, blue; O, red; Zn, lavender; H omitted for clarity. Reproduced from Ref. [49] published by The Royal Society of Chemistry (2015). (Color online.)

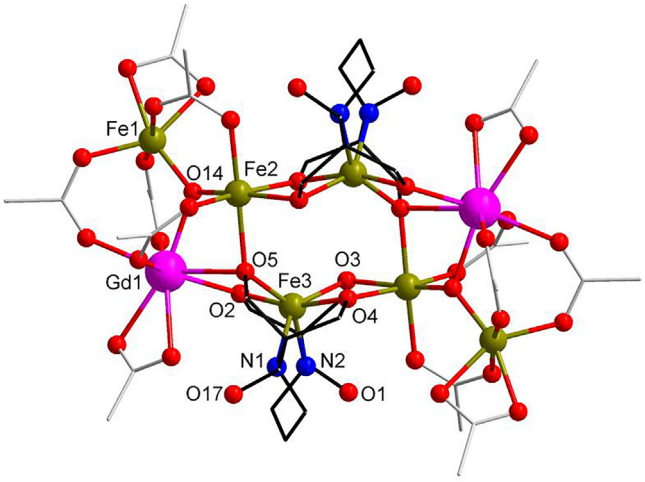

Fig. 9. Structure of $[Fe_6Gd_2(O)_2(H_2L)_2(Piv)_{12}]$ C, grey; Fe, green; Gd, pink; N, blue; O, red; H and Me groups of the pivalate ligands omitted for clarity. Image created from the crystallographic information file (CIF) from the Cambridge Structural Database (CSD) Refcode: XUGYEF. (Color online.)

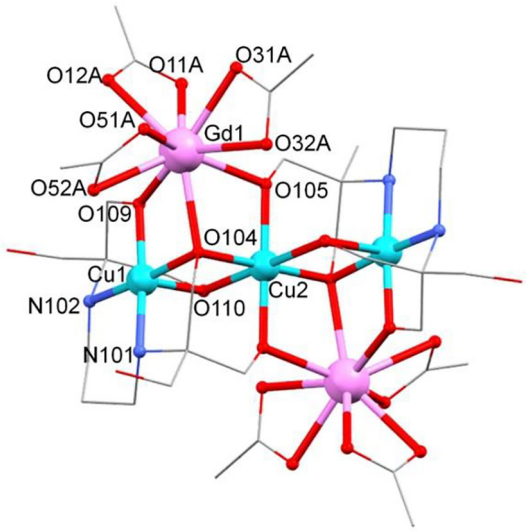

Fig. 10. Structure of $[Gd_2Cu_3(H_3L)_2(OAc)_6]$. C, grey; Cu, turquoise; Gd, pink; N, blue; O, red; H omitted for clarity. Reprinted with permission from Ref. [55]. Copyright 2016 Wiley-VCH. (Color online.)

$[Fe_3O(Piv)_6(H_2O)_3]\cdot Piv$ (Piv^- = pivalate, $Me_3CCO_2^-$) with $Ln(NO_3)_3$ and LiOH in EtOH/DMF (solvothermal to 90 °C for 48 h followed by controlled slow cooling). This is similar to the oxo-centered triangle route used to prepare the Fe_{10} complex **1**, but instead using a solvothermal reaction as for the Dy_4 complex **6**. The central portion of the structure consists of two iron(III) centers, each encapsulated by a Bis-tris propane H_2L^{4-} ligand in a $\{N_2O_4\}$ donor set (Chart 2, Fig. 9). These centers are in a less common distorted trigonal prismatic geometry (*c.f.* Fe_{10} distorted mono-capped trigonal prism) and bridge two Fe_2Ln triangles in a similar way to the Fe_{10} complex, which bridges two Fe_4 butterfly units. Again a carboxylate co-ligand is required to help assemble the structure. The Dy(III) and Tb(III) analogues show the onset of slow magnetic relaxation at low temperature but no peaks are observed in the out-of-phase AC susceptibility.

In the Cu/Mn and Cu/Zn heterometallic complexes with Bis-tris propane, the Cu(II) centers occupy the internal $\{N_2O_2\}$ pocket of the ligand to the detriment of other 3d ions present in the reaction media [53], and thus the ligand exerts a level of control over the final molecular assembly. Furthermore, Cu(II) ions display a flexible coordination geometry and a strong tendency for ferromagnetic Cu···4f interactions for the heavier Ln ions [54]. The reaction of Cu $(OAc)_2$ with H_6L and Et_3N in MeOH followed by addition of Ln $(OAc)_3$ (Ln = Gd(III), Tb(III)) with heating gives $[Ln_2Cu_3(H_3L)_2(OAc)_6]$ (Ln = Gd (**16**), Tb (**17**)) after vapor diffusion with THF [55]. Similar reactions using nitrate salts and NMe_4OH results in a slightly different series of Cu/4f complexes with formula $(NMe_4)_2[Gd_2Cu_3(H_3L)_2(NO_3)_8(EtOH)_2]$ (**18**), or $(NMe_4)_2[Ln_2Cu_3(H_3L)_2(NO_3)_7(MeOH)_2](NO_3)$ (Ln = Tb (**19**), Dy (**20**), Ho (**21**), Er (**22**) from slow evaporation.

The structures of **16** and **17** contain two Ln(III) ions coordinated to a $\{Cu_3(H_3L)_2\}$ linear unit through two triply deprotonated H_3L^{3-} ligands (Fig. 10). The two external Cu(II) ions of the linear unit are encapsulated by two μ_4-H_3L^{3-} ligands through O, N-donor atoms (Chart 2) in a distorted square-pyramidal geometry. The two remaining hydroxyl arms on each ligand which do not bridge metal ions are uncoordinated. The Ln(III) ions are in a spherical capped square antiprismatic geometry (C_{4v}). The replacement of acetate for nitrate anions decreases the symmetry within the molecule and promotes different coordination environments around the metal ions present in the structure (Fig. 11). Consequently, the structure of $(NMe_4)_2[Tb_2Cu_3(H_3L)_2(NO_3)_7(MeOH)_2](NO_3)$ (**19**) contains a $\{Cu_3(H_3L)_2\}$ linear unit linked to two Tb(III) ions as seen

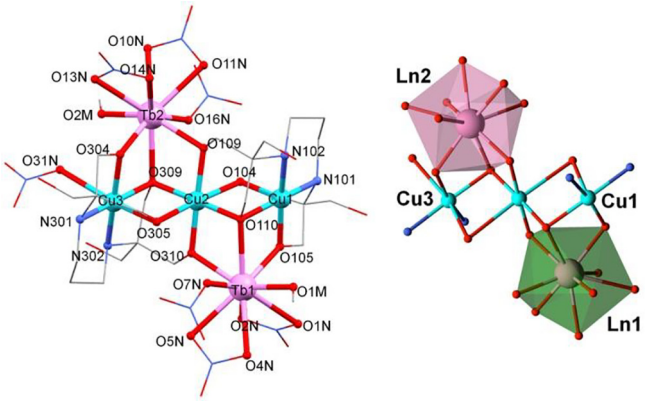

Fig. 11. Structure of the anion (left) and detail of the metal alkoxide core (right) in $(NMe_4)_2[Tb_2Cu_3(H_3L)_2(NO_3)_7(MeOH)_2](NO_3)$ (**19**). C, grey; Cu, turquoise; Tb, pink; N, blue; O, red; H omitted for clarity. Polyhedra around Ln(III) ions are highlighted in green (Ln1, C_s) and pink (Ln2, C_{4v}). Reprinted with permission from Ref. [55]. Copyright 2016 Wiley-VCH. (Color online.)

in **17**, but here the H_3L^{3-} ligands are coordinated to Cu(II) centers which have two different geometries. As shown in Fig. 11, Cu1 is in a [4 + 1] distorted square-based pyramidal geometry and Cu3 is in a distorted octahedral geometry due to the coordination of an additional monodentate NO_3^- ligand. The central Cu(II) ion displays the distorted octahedral geometry seen in **17**. Two bidentate and one monodentate NO_3^- ligands, plus one MeOH ligand complete the coordination environment of each nona-coordinated Tb(III) center. Tb2 is in a spherical capped square antiprism environment (C_{4v})) (Fig. 11, right), whereas Tb1 displays a muffin geometry (C_s).

All of the $\{Ln_2Cu_3\}$ complexes display ferromagnetic coupling. The susceptibility and magnetization data for $[Gd_2Cu_3(H_3L)_2(OAc)_6]$ (**16**) were fitted simultaneously to give $J_{Cu\cdots Gd}$ = +1.8 cm^{-1}, $J_{Cu\cdots Cu}$ = +69.7 cm^{-1} (with $\hat{H} = -2J$ notation). For $(NMe_4)_2[Gd_2Cu_3(H_3L)_2(NO_3)_8(EtOH)_2]$ (**18**) this gives $J_{Cu\cdots Gd}$ = +1.9 cm^{-1}, and a weaker $J_{Cu\cdots Cu}$ = +16.7 cm^{-1}, which could be due to increased Cu(II)···Cu(II) distances and larger Cu-μ_3O-Cu′ bridging angles. $[Tb_2Cu_3(H_3L)_2(OAc)_6]$ (**17**) displays slow magnetic relaxation in AC studies and analysis yields $\tau_0 = 1.3 \cdot 10^{-7}$ s and $\Delta E/k_B$ = 21.4 ± 0.5 K. The AC studies for **19**–**22** reveal slow magnetic relaxation

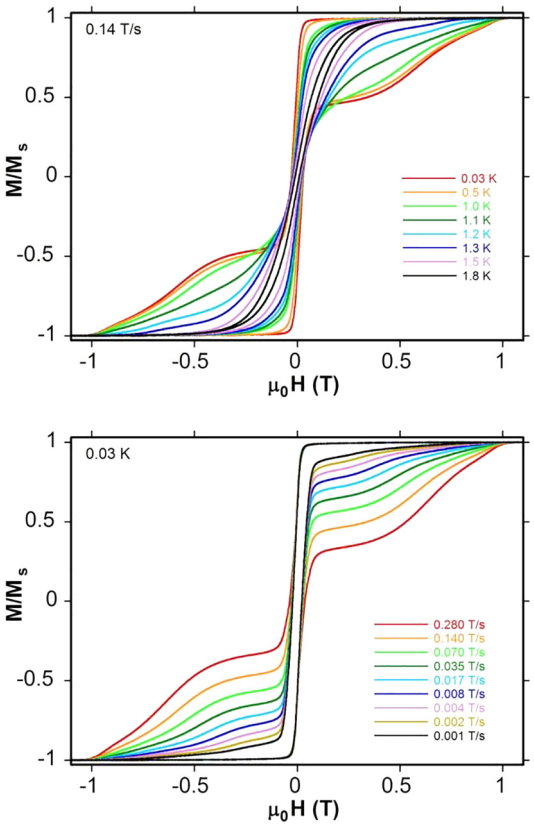

Fig. 12. Single-crystal magnetization *vs.* field hysteresis loops for **19**: with a constant field-sweep rate of 0.14 T s^{-1} at different temperatures between 0.03 K and 1.8 K (top); at a constant temperature of 0.03 K with different sweep rates between 0.001 T s^{-1} and 0.280 T s^{-1} (bottom). Reprinted with permission from Ref. [55]. Copyright 2016 Wiley-VCH.

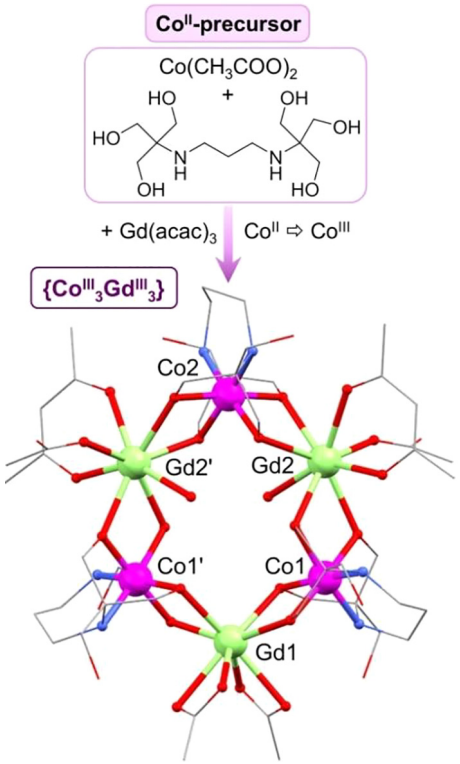

Fig. 13. Synthetic approach and structure of $[Co^{III}_3Gd^{III}_3(H_2L)_3(acac)_2(OAc)_4(H_2O)_2]$. C, grey; Co, fuchsia; Gd, green; N, blue; O, red; hydrogen atoms and solvent molecules are omitted for clarity. Reproduced from Ref. [57] published by The Royal Society of Chemistry (2017). (Color online.)

and analysis of this data for $(NMe_4)_2[Tb_2Cu_3(H_3L)_2(NO_3)_7(MeOH)_2](NO_3)$ (**19**) yields $\tau_0 = 1.0{\cdot}10^{-7}$ s and $\Delta E/k_B = 36.0 \pm 0.2$ K. There is a decrease of the effective barrier along the lanthanide series, with **19** showing the highest $\Delta E/k_B$ value, and **22** showing the lowest. The substitution of the three chelating acetate ligands for two chelating nitrates, one monodentate nitrate and one MeOH ligand leads to a ~70% improvement of the effective energy barrier (21.4 K for **17**, 36.0 K for **19**). Complex **19** shows SMM-typical sweep-rate-dependent hysteresis curves with non-zero coercivity and a large step at around zero magnetic field induced by resonant spin ground state tunneling (Fig. 12). To understand the large barrier height observed for the Tb analogues and to probe the origin of the differences in the barrier height, mononuclear Tb(III) complexes derived from the X-ray structures of complexes **17** and **19** were modeled using *ab initio* CASSCF calculations. For **17** a significant tunnel splitting (Δ_{tun}) is observed within the ground multiplet (0.45 cm^{-1}), but this is quenched by both Cu···Cu and Cu···Tb interactions as they behave like an internal applied field, leading to the observation of zero-field SMM behavior. For complex **19**, the tunnel splitting within the ground multiplet is small for the Tb(III) center with C_s symmetry (0.08 cm^{-1}) and significant for the other center with C_{4v} symmetry (0.32 cm^{-1}). Although the chemical environments of the ligands are different, the computational models suggest that the improvement in the magnetic behavior going from complex **17** to complex **19** is due to a reduction in the tunnel splitting for the Tb(III) ion in **19** in the C_s symmetry environment.

The Cu/Ln systems led us to explore the chemistry of Bis-tris propane with other 3d/4f combinations. A large magnetocaloric effect (MCE) at low temperatures is favored by a negligible magnetic anisotropy and several molecule-based refrigerants are complexes of isotropic Gd(III) ions. Although Co/Gd complexes have been studied in search of the enhancement of magnetocaloric properties [56], Co(II) ions have a negative influence, because of the characteristic large magnetic anisotropy, which makes reorientation of the magnetic moment more difficult. Our approach to Co/Gd systems for MCE used $\{Co^{II}(H_6L)\}$ precursors which undergo facile oxidation to diamagnetic Co(III) [57]. Importantly, the Co(III) ions have a significant impact on the adiabatic temperature change, by separating the Gd(III) ions and weakening the Gd(III)···Gd(III) interactions. Combining $[Co(H_6L)(OAc)_2]$ and $Gd(acac)_3$ in MeCN/MeOH under aerobic conditions with heating produces $[Co^{III}_3Gd^{III}_3(H_2L)_3(acac)_2(OAc)_4(H_2O)_2]$ (**23**). The pre-formation of the metallo-ligand seems to be essential for the assembly, as previously seen for the $\{Mn_{18}Cu_6\}$ complexes. The structure contains three octahedral Co(III) ions, each one encapsulated by one tetradeprotonated H_2L^{4-} ligand (Fig. 13), with two remaining ligand arms uncoordinated (Chart 2). Each $\{Co(H_2L)\}$ unit is linked to two triangular dodecahedral Gd(III) ions through four μ-O bridging atoms forming a ring-like structure, in which Co(III) and Gd(III) centers alternately occupy the corners of a six-pointed star.

The $\{Co^{III}_3Gd^{III}_3\}$ structure is the smallest member of a family of alternating 3d/4f rings (where 3d = Mn or Fe only), such as $\{Mn_4Ln_4\}$, $\{Mn_8Ln_8\}$ or $\{Fe_{10}Yb_{10}\}$ which are all more puckered than **23** [19,58,59,60].

The DC magnetic measurements suggest that **23** should display a relatively large MCE, arising from the weakly-interacting Gd(III) ions, which are well separated by the diamagnetic Co(III) centers. For the largest applied field change B = (7–0) T, *i.e.*, after a full demagnetization from 7 T, the maximum value of the magnetic entropy change $-\Delta S_m$ is 23.6 J kg^{-1} K^{-1} per unit mass. In terms of the magnetocaloric properties, the diamagnetic Co(III) ions have a negative influence on the entropy change per unit mass: the

lower the magnetic/non-magnetic ions ratio, the lower are the magnetic heat capacity and entropy per unit mass. However, the key point is that the Co(III) centers have a positive impact on the adiabatic temperature change ΔT_{ad}. The intermediate presence of the Co(III) ions weakens the magnetic interaction between the Gd(III) ions, so the temperature-dependence of ΔT_{ad} has a maximum at a relatively lower temperature than usually found for homometallic Gd(III) complexes (ΔT_{ad} = 10.7 K at T = 1.5 K). Among the few known systems that have a ΔT_{ad} maximum below *e.g.,* 2 K for 7 T, complex **23** lags behind only the extraordinary {Gd_2-ac} with ΔT_{ad} = 12.6 K at T = 1.4 K [61], while it outdoes {Zn_2-Gd_2} with ΔT_{ad} = 9.6 K at T = 1.4 K [62], and {Gd_7} with ΔT_{ad} = 9.4 K at T = 1.8 K [6].

5. Synopsis

The majority of the polymetallic complexes isolated so far that contain the Bis-tris propane ligand (H_6L) contain additional simple chelating co-ligands such as carboxylates or β-diketonates and in terms of magnetic properties, the 3d/4f {Cu_3Tb_2} and {Co_3Gd_3} complexes are the most impressive. The flexibility of ligand binding mode highlighted in Chart 2 is quite incredible given that relatively few polymetallic complexes containing the ligand have been isolated. The most common level of ligand deprotonation in the complexes is H_2L^{4-} and a higher level of deprotonation has not been observed. Often the two remaining ligand OH groups provide hydrogen bonding interactions in the lattice. The ligand binds *via* an {N_2O_4} donor set with Fe(III), Mn(III), Co(III) and Dy(III); {N_2O_3} with Ni(II); {N_2O_2} or {N_2O_3} with Cu(II) and {N_2O_2} with V(IV) in a hybrid polyoxovanadate complex. There are some obvious targets in terms of chemistry: from the 3d ions, binding to chromium has not been reported; for homometallic lanthanide complexes, only one Dy(III) complex has been reported and for heterometallic complexes, only Cu/Zn and Cu/Mn (for 3d, 3d′) and Fe/Ln; Cu/Ln and Co/Ln complexes (for 3d/4f) have been reported. So far, the most spectacular structures have been isolated in the absence of co-ligands, *i.e.* the two {$Mn_{18}Cu_6$} complexes with three different polyhedral shells and the {Cu_8Zn_8} double-concentric ring structure and it is likely that further large heterometallic complexes could be synthesized by employing Bis-tris propane as the sole polydentate organic ligand.

Acknowledgements

The UK Engineering and Physical Sciences Research Council (EP/I027203/1) and The University of Glasgow are thanked for financial support. Our development of the coordination chemistry of Bis-tris propane as a new polydentate ligand for high nuclearity homo- and heterometallic complexes would not have been possible without the hard work of a handful of very talented coordination chemists: Dr. Alan Ferguson; Dr. Vicki Milway and Dr. María José Heras Ojea. Furthermore, we are indebted to our collaborators and their co-workers who have carried out measurements or calculations on these systems: Dr. Andy Parkin; Dr. Marc Schmidtmann; Dr. Lynne Thomas; Prof. Simon Parsons; Dr. Claire Wilson; Dr. Floriana Tuna; Prof. Wolfgang Wernsdorfer; Prof. Marco Evangelisti and Prof. Gopalan Rajaraman.

References

[1] C. Papatriantafyllopoulou, E.E. Moushi, G. Christou, A.J. Tasiopoulos, Chem. Soc. Rev. 45 (2016) 1597.
[2] X.-Y. Zheng, Y.-H. Jiang, G.-L. Zhuang, D.-P. Liu, H.-G. Liao, X.-J. Kong, L.-S. Long, L.-S. Zheng, J. Am. Chem. Soc. 139 (2017) 18178.
[3] G.F.S. Whitehead, F. Moro, G.A. Timco, W. Wernsdorfer, S.J. Teat, R.E.P. Winpenny, Angew. Chem. Int. Ed. 52 (2013) 9932.
[4] M. Manoli, S. Alexandrou, L. Pham, G. Lorusso, W. Wernsdorfer, M. Evangelisti, G. Christou, A.J. Tasiopoulos, Angew. Chem. Int. Ed. 55 (2016) 679.
[5] J. Ferrando-Soria, J. Vallejo, M. Castellano, J. Martínez-Lillo, E. Pardo, J. Cano, I. Castro, F. Lloret, R. Ruiz-García, M. Julve, Coord. Chem. Rev. 339 (2017) 17.
[6] E. Moreno Pineda, G. Lorusso, K.H. Zangana, E. Palacios, J. Schnack, M. Evangelisti, R.E.P. Winpenny, E.J.L. McInnes, Chem. Sci. 7 (2016) 4891.
[7] J. Ferrando-Soria, E. Moreno Pineda, A. Chiesa, A. Fernandez, S.A. Magee, S. Carretta, P. Santini, I.J. Vitorica-Yrezabal, F. Tuna, G.A. Timco, E.J.L. McInnes, R. E.P. Winpenny, Nat. Commun. 7 (2016) 11377.
[8] K.R. Vignesh, A. Soncini, S.K. Langley, W. Wernsdorfer, K.S. Murray, G. Rajaraman, Nat. Commun. 8 (2017) 1023.
[9] M.A. Palacios, E. Moreno Pineda, S. Sanz, R. Inglis, M.B. Pitak, S.J. Coles, M. Evangelisti, H. Nojiri, C. Heesing, E.K. Brechin, J. Schnack, R.E.P. Winpenny, ChemPhysChem 17 (2016) 55.
[10] A.B. Canaj, M. Siczek, T. Lis, M. Murrie, E.K. Brechin, C.J. Milios, Dalton Trans. 46 (2017) 7677.
[11] L. Qin, G.-J. Zhou, Y.-Z. Yu, H. Nojiri, C. Schröder, R.E.P. Winpenny, Y.-Z. Zheng, J. Am. Chem. Soc. 139 (2017) 16405.
[12] A. Cini, M. Mannini, F. Totti, M. Fittipaldi, G. Spina, A. Chumakov, R. Rüffer, A. Cornia, R. Sessoli, Nat. Commun. 9 (2018) 480.
[13] M. Mahdi Najafpour, G. Renger, M. Hołyńska, A. Nemati Moghaddam, E.-M. Aro, R. Carpentier, H. Nishihara, J.J. Eaton-Rye, J.-R. Shen, S.I. Allakhverdiev, Chem. Rev. 116 (2016) 2886.
[14] G. Maayan, N. Gluz, G. Christou, Nat. Catal. 1 (2018) 48.
[15] G. Guthausen, J.R. Machado, B. Luy, A. Baniodeh, A.K. Powell, S. Krämer, F. Ranzinger, M.P. Herrling, S. Lacknere, H. Horne, Dalton Trans. 44 (2015) 5032.
[16] F.J. Douglas, D.A. MacLaren, N. Maclean, I. Andreu, F.J. Kettles, F. Tuna, C.C. Berry, M. Castro, M. Murrie, RSC Adv. 6 (2016) 74500.
[17] S.M. Lewis, A. Fernandez, G.A. DeRose, M.S. Hunt, G.F.S. Whitehead, A. Lagzda, H.R. Alty, J. Ferrando-Soria, S. Varey, A.K. Kostopoulos, F. Schedin, C.A. Muryn, G.A. Timco, A. Scherer, S.G. Yeates, R.E.P. Winpenny, Angew. Chem., Int. Ed. 56 (2017) 6749.
[18] M. Coletta, R. McLellan, S. Sanz, K.J. Gagnon, S.J. Teat, E.K. Brechin, S.J. Dalgarno, Chem. Eur. J. 23 (2017) 14073.
[19] A. Baniodeh, N. Magnani, Y. Lan, G. Buth, C.E. Anson, J. Richter, M. Affronte, J. Schnack, A.K. Powell, Npj Quantum Mater. 3 (2018) 10.
[20] K.J. Mitchell, K.A. Abboud, G. Christou, Nat. Commun. 8 (2017) 1445.
[21] C.J. Milios, R.E.P. Winpenny, Struct. Bonding 164 (2015) 1.
[22] J.A. Sheikh, H.S. Jena, A. Clearfield, S. Konar, Acc. Chem. Res. 49 (2016) 1093.
[23] H.-Y. Zang, J.-J. Chen, D.-L. Long, L. Cronin, H.N. Miras, Adv. Mater. 25 (2013) 6245.
[24] R.E.P. Winpenny, Chem. Soc. Rev. 27 (1998) 447.
[25] A. Ferguson, A. Parkin, J. Sanchez-Benitez, K. Kamenev, W. Wernsdorfer, M. Murrie, Chem. Commun. (2007) 3473.
[26] A. Ferguson, J. McGregor, E.K. Brechin, L.H. Thomas, M. Murrie, Dalton Trans. (2009) 9395.
[27] A. Ferguson, A. Parkin, M. Murrie, Dalton Trans. (2006) 3627.
[28] A. Ferguson, J. McGregor, A. Parkin, M. Murrie, Dalton Trans. (2008) 731.
[29] K. Graham, L.E. Sharp, L.H. Thomas, M. Murrie, Inorg. Chem. Commun. 25 (2012) 89.
[30] T. Laureys, I.S.S. Pinto, C.V.M. Soares, H.B. Boppudi, H.M.V.M. Soares, Chem. Eng. Data 57 (2012) 87.
[31] S.S. Deshmukh, C. Protheroe, M.-A. Ivanescu, S. Lag, L. Kálmán, BBA – Bioenergetics 1859 (2018) 227.
[32] D.E. Williams, K. Basnet, K.B. Grant, ChemBioChem 16 (2015) 1474.
[33] A.F. Eftaiha, A.K. Qaroush, K.I. Assaf, F. Alsoubani, T.M. Pehl, C. Troll, M.I. El-Barghouthia, New. J. Chem. 41 (2017) 11941.
[34] A. Ferguson, A. Darwish, K. Graham, M. Schmidtmann, A. Parkin, M. Murrie, Inorg. Chem. 47 (2008) 9742.
[35] C. Cañada-Vilalta, E. Rumberger, E.K. Brechin, W. Wernsdorfer, K. Folting, E.R. Davidson, D.N. Hendrickson, G. Christou, J. Chem. Soc., Dalton Trans. (2002) 4005.
[36] A. Ferguson, M. Schmidtmann, E.K. Brechin, M. Murrie, Dalton Trans. 40 (2011) 334.
[37] B.-W. Qin, K.-C. Huang, Y. Zhang, L. Zhou, Z. Cui, K. Zhang, X.-Y. Zhang, J.-P. Zhang, Chem. Eur. J. 24 (2018) 1962.
[38] O. Nachtigall, A. Hagenbach, J. Wiecko, D. Lentz, U. Abram, J. Spandl, Dalton Trans. 46 (2017) 509.
[39] P. Gómez-Tagle, A.K. Yatsimirsky, Inorg. Chem. 40 (2001) 3786.
[40] L. Rosado Piquera, E. Carolina Sañudo, Dalton Trans. 44 (2015) 8771.
[41] W.-P. Chen, P.-Q. Liao, Y. Yu, Z. Zheng, X.-M. Chen, Y.-Z. Zheng, Angew. Chem. Int. Ed. 55 (2016) 9375.
[42] V.A. Milway, F. Tuna, A.R. Farrell, L.E. Sharp, S. Parsons, M. Murrie, Angew. Chem. Int. Ed. 52 (2013) 1949.
[43] M.V. Kirillova, C.I.M. Santos, V. André, T.A. Fernandes, S.S.P. Diasa, A.M. Kirillov, Inorg. Chem. Front. 4 (2017) 968.
[44] Z. Sun, P.K. Gantzel, D.N. Hendrickson, Inorg. Chem. 35 (1996) 6640.
[45] L. Zhang, R. Clérac, P. Heijboer, W. Schmitt, Angew. Chem., Int. Ed. 51 (2012) 3007.
[46] A. Saha, K.A. Abboud, G. Christou, Inorg. Chem. 50 (2011) 12774.
[47] Y.-X. Wang, W. Shi, H. Li, Y. Song, L. Fang, Y. Lan, A.K. Powell, W. Wernsdorfer, L. Ungur, L.F. Chibotaru, M. Shen, P. Cheng, Chem. Sci. 3 (2012) 3366.
[48] J.M. Frost, F.J. Kettles, C. Wilson, M. Murrie, Dalton Trans. 45 (2016) 18094.
[49] M. Heras Ojea, C. Wilson, S.J. Coles, F. Tuna, M. Murrie, Dalton Trans. 44 (2015) 19275.

[50] S.K. Langley, D.P. Wielechowski, V. Vieru, N.F. Chilton, B. Moubaraki, B.F. Abrahams, L.F. Chibotaru, K.S. Murray, Angew. Chem., Int. Ed. 52 (2013) 12014.
[51] K.R. Vignesh, S.K. Langley, K.S. Murray, G. Rajaraman, Chem. Eur. J. 23 (2017) 1654.
[52] S.-D. Han, S.-J. Liu, Q.-L. Wang, X.-H. Miao, T.-L. Hu, X.-H. Bu, Cryst. Growth Des. 15 (2015) 2253.
[53] H. Li, B. Shao, Y. Li, L. Chen, J. Zhao, Inorg. Chem. Commun. 61 (2015) 68.
[54] C. Benelli, D. Gatteschi, Chem. Rev. 102 (2002) 2369.
[55] M. Heras Ojea, V.A. Milway, G. Velmurugan, L.H. Thomas, S.J. Coles, C. Wilson, W. Wernsdorfer, G. Rajaraman, M. Murrie, Chem. Eur. J. 22 (2016) 12839.
[56] Y.-Z. Zheng, M. Evangelisti, F. Tuna, R.E.P. Winpenny, J. Am. Chem. Soc. 134 (2012) 1057.
[57] M. Heras Ojea, G. Lorusso, G.A. Craig, C. Wilson, M. Evangelisti, M. Murrie, Chem. Commun. 53 (2017) 4799.
[58] M. Li, A.M. Ako, Y. Lan, W. Wernsdorfer, G. Buth, C.E. Anson, A.K. Powell, Z. Wang, S. Gao, Dalton Trans. 39 (2010) 3375.
[59] A. Baniodeh, C.E. Anson, A.K. Powell, Chem. Sci. 4 (2013) 4354.
[60] K.R. Vignesh, S.K. Langley, B. Moubaraki, K.S. Murray, G. Rajaraman, Chem. Eur. J. 21 (2015) 16364.
[61] M. Evangelisti, O. Roubeau, E. Palacios, A. Camón, T.N. Hooper, E.K. Brechin, J.J. Alonso, Angew. Chem., Int. Ed. 50 (2011) 6606.
[62] J. Ruiz, G. Lorusso, M. Evangelisti, E.K. Brechin, S.J.A. Pope, E. Colacio, Inorg. Chem. 53 (2014) 3586.